



Two-Dimensional Directional Proton Emission in Dissociative Ionization of H₂

Xiaochun Gong,¹ Peilun He,^{2,3} Qiying Song,¹ Qinying Ji,¹ Haifeng Pan,¹ Jingxin Ding,¹ Feng He,^{3,*}
Heping Zeng,^{1,4,†} and Jian Wu^{1,‡}

¹State Key Laboratory of Precision Spectroscopy, East China Normal University, Shanghai 200062, China

²School of Agriculture and Biology, Shanghai Jiao Tong University, Shanghai 200240, China

³Key Laboratory of Laser Plasmas (Ministry of Education) and Department of Physics and Astronomy, Shanghai Jiao Tong University, Shanghai 200240, China

⁴Synergetic Innovation Center of Quantum Information and Quantum Physics, University of Science and Technology of China, Hefei, Anhui 230026, China

(Received 4 June 2014; published 12 November 2014)

An intense phase-controlled orthogonally polarized two-color ultrashort laser pulse is used to singly ionize and dissociate H₂ into a neutral hydrogen atom and a proton. Emission-direction and kinetic-energy dependent asymmetric dissociation of H₂ is observed as a function of the relative phase of the orthogonally polarized two-color pulse. Significant asymmetric proton emission is measured in the direction between two polarization axes. Our numerical simulations of the time-dependent Schrödinger equation reproduce many of the observed features. The asymmetry is attributed to the coherent superposition of two-dimensional nuclear wave packets with opposite parities, which have the same energies and overlap in the same emission directions.

DOI: 10.1103/PhysRevLett.113.203001

PACS numbers: 33.80.Rv, 34.80.Ht, 42.50.Hz, 42.65.Re

Directional molecular bond breaking, as the key ingredient for the coherent control of chemical reactions [1,2], has attracted much attention in past decades. Intense phase-controlled near-infrared few-cycle [3–7] or two-color laser pulses [8–13] of symmetry-broken electric waveforms have been used to control the directional dissociative ionization of molecules. The underlying physics [14–18] is understood as either the quantum interference of the nuclear wave packets of opposite parities or the classical localization of the remaining electron. A modest near-infrared laser pulse is effective to steer the intramolecular motion of the electron until its localization at one of the departing nuclei after the ultrafast ionization induced by an ultraviolet attosecond pulse [19–21]. It is the phase of the laser field at the ionization instant that governs the directional dissociative ionization of the molecule in the laser pulse as probed by the technique of coincidence angular streaking [22]. This directional bond breaking was recently experimentally demonstrated in the photodissociation of a molecular-ion target [23,24] by using a phase-controlled near-infrared few-cycle laser pulse, which avoided the first ionization step and thus could be qualitatively compared with quantum simulations.

However, almost all of the foregoing directional dissociation controls were demonstrated in a one-dimensional stage along the direction of field polarization [3–24]. The control of the directional bond breaking rapidly diminishes for the molecule oriented away from the polarization axis of the dissociation field [4,24]. Here, we report two-dimensional directional dissociative ionization of H₂ by using an intense phase-controlled

orthogonally polarized two-color (OTC) laser pulse. It stands for a two-dimensional pathway interference of the nuclear wave packets with opposite parities. Bright butterfly structure is observed in the proton momentum distribution owing to conjunct driving of the orthogonally polarized fundamental (FW) and second-harmonic (SH) waves. By tuning the relative phase of the OTC pulse, we find significant asymmetric proton emission in the direction between the polarization axes of the two colors, which varies as the kinetic energy of the proton due to the interference of different dissociation pathways. By numerically propagating a two-dimensional nuclear wave packet in the OTC pulse, we observe similar angle-resolved asymmetries.

We produce the phase-controlled OTC laser pulse in a collinear scheme [13]. An FW pulse (25 fs, 790 nm, 10 kHz, polarized along the *z* axis) from a multipass amplification Ti:sapphire laser system is down-collimated into a 150- μ m-thick β -barium borate (BBO) crystal to produce an SH pulse at 395 nm (polarized along the *y* axis). The time lag between the FW and SH pulses is compensated with a birefringent α -BBO crystal. A pair of fused-silica wedges is used to finely tune the relative phase, ϕ_L , between the FW and SH waves of the OTC pulse, whose absolute value is calibrated by analyzing the directional dissociative ionization of CO molecules [13]. As illustrated in Fig. 1(a), the generated OTC laser pulse is sent into a standard reaction microscope of cold target recoil ion momentum spectroscopy setup [25,26] and focused onto a supersonic gas jet of H₂ by a concave mirror ($f = 7.5$ cm) inside the chamber. The intensities of the

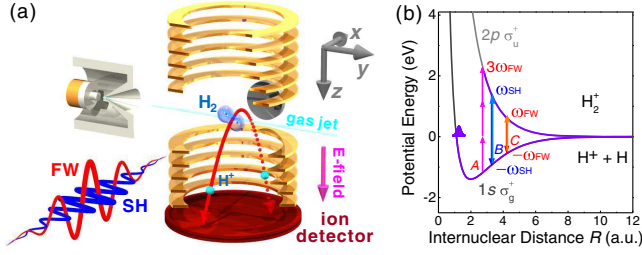


FIG. 1 (color online). (a) Schematic diagram of the experiment apparatus. The OTC pulse propagates along the x axis is backfocused by a concave mirror onto the molecular beam propagating along the y axis. The emitted H^+ is guided by a weak electric field (pink arrow) and measured by a time- and position-sensitive detector at the end of the spectrometer. The FW and SH waves of the OTC pulse polarize along the z and y axes, respectively. (b) The potential energy curves of H_2^+ as a function of the internuclear distance R and the possible dissociation pathways in the two-color field. Here, a.u. refers to the atomic units throughout unless otherwise stated.

FW and SH fields in the reaction region are measured to be $I_{0,FW} \sim 8.3 \times 10^{13}$ and $I_{0,SH} \sim 6.0 \times 10^{12}$ W/cm², respectively. The OTC pulse first singly ionizes H_2 to H_2^+ which then dissociates into a neutral hydrogen atom H and a proton H^+ . The positively charged proton is guided by a weak homogeneous electric field and detected by a time- and position-sensitive microchannel plate detector [27] at the end of the spectrometer. The three-dimensional momentum vectors of the proton are reconstructed from the measured time-of-flights and positions of the fragment ion. We restrict our data analysis and discussion to protons ejected in the polarization plane of the OTC pulse where the molecules mostly dissociate. We rule out the contribution of the excited neutral fragment of H^* (e.g., in the Rydberg state) [28,29] to the observed directional proton emission which is difficult to be generated by our OTC pulse and out of the time-of-flight range of interest in our analysis.

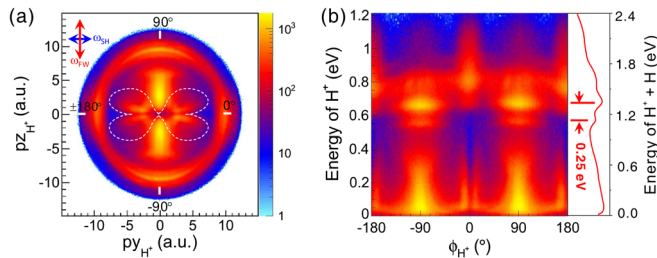


FIG. 2 (color online). (a) The momentum distribution of the emitted H^+ from the dissociative single ionization of H_2 in the polarization plane of the OTC pulse. The butterfly structure of the H^+ is indicated by a dashed curve. (b) The kinetic-energy distribution of the H^+ versus its emission direction ϕ_{H^+} . The right panel shows the yield of H^+ as a function of the total kinetic energy of H^+ and H . Logarithm scale is used here.

Figure 2(a) shows the momentum distribution of H^+ in the polarization y - z plane of the OTC pulse integrated over all the laser phase of ϕ_L . The corresponding kinetic energy of H^+ , E_k , versus the ion-emission direction, ϕ_{H^+} , is plotted in Fig. 2(b). It shows a rich structure as a function of ϕ_{H^+} . The potential dissociation pathways in the OTC field are illustrated in Fig. 1(b). The H^+ ejecting along the FW polarization axis near $\phi_{H^+} = \pm 90^\circ$ at low ($E_k < 0.4$ eV) and high kinetic energies (0.5 eV $< E_k < 1.2$ eV) originate from the $1\omega_{FW}$ (propagation on the $1s\sigma_g^+$ curve undergoes one- ω_{FW} -photon transition to the $2p\sigma_u^+$ curve at point C, followed by dissociation along the $2p\sigma_u^+$ curve) and net- $2\omega_{FW}$ (propagation on the $1s\sigma_g^+$ curve undergoes three- ω_{FW} -photon transition to the $2p\sigma_u^+$ curve at point A, followed by propagation on the $2p\sigma_u^+$ curve and coupling back to the $1s\sigma_g^+$ curve at point C by emitting one photon of ω_{FW} , followed by dissociation along the $1s\sigma_g^+$ curve) dissociation pathways, respectively. On the other hand, the H^+ ejecting along the SH polarization axis near $\phi_{H^+} = 0^\circ$ or $\pm 180^\circ$ at high kinetic energy (0.5 eV $< E_k < 1.2$ eV) originates from the $1\omega_{SH}$ dissociation pathway (propagation on the $1s\sigma_g^+$ curve undergoes one- ω_{SH} -photon transition to the $2p\sigma_u^+$ curve at point B, followed by dissociation along the $2p\sigma_u^+$ curve). Interestingly, as shown in Fig. 2(b), a fine structure is clearly resolved in the high-kinetic-energy region of the proton spectrum. By considering the kinetic energy of the undetected neutral H from the dissociative ionization of H_2 , as plotted in the right panel of Fig. 2(b), the energy space of 0.25 eV in the total kinetic energy corresponds to the vibrational interval of the ground electronic state of H_2^+ (e.g., $E_{v=1} - E_{v=0} \sim 0.25$ eV). The dipole-transition induced photodissociation thus allows us to resolve the vibrational states of H_2^+ in complex strong-field dissociative ionization.

However, the H^+ ejecting in the direction between the polarization axes, e.g., the butterfly structure indicated by the dashed curve in Fig. 2(a), is caused by the conjunct driving of the FW and SH waves of the OTC pulse. This is verified experimentally by scanning the time delay between the FW and SH pulses. To do that, the FW and SH waves are separated from the OTC pulse and then latterly recombined by dichromatic mirrors with a motorized delay stage in the SH arm. As shown in Fig. 3(a), the butterfly structure emerges only when two pulses are overlapped. Since the SH pulse is too weak to ionize H_2 , no H^+ near $\phi_{H^+} = 0^\circ$ or $\phi_{H^+} = \pm 180^\circ$ is observed when the SH pulse is temporally advanced with respect to the FW pulse [see Fig. 3(b)]. The H^+ emitting to $\phi_{H^+} = \pm 90^\circ$ in Fig. 3(b) is produced solely by the FW pulse. On the other hand, when the SH pulse is temporally behind the FW pulse, H^+ near $\phi_{H^+} = 0^\circ$ or $\phi_{H^+} = \pm 180^\circ$ is also observed in addition to that near $\phi_{H^+} = \pm 90^\circ$ [see Fig. 3(c)]. As compared to the dipole transition induced dissociation, the single ionization rate of H_2 weakly depends on the molecular orientation with respect to the laser polarization [30]. The weak SH

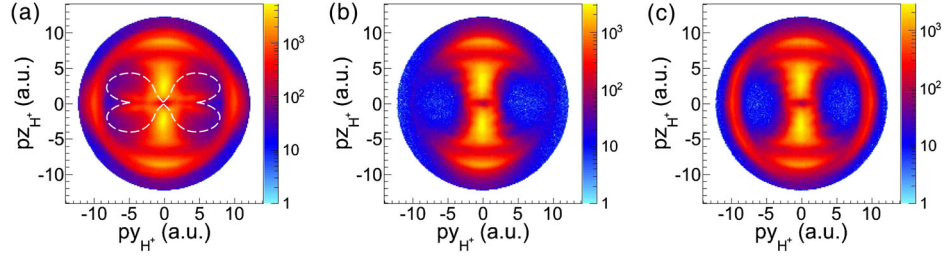


FIG. 3 (color online). The momentum distributions of H^+ in the y - z plane as a function of the time delay (T_{delay}) between the orthogonally polarized FW and SH pulses. The SH pulse is tuned to be temporally (a) overlapped ($T_{\text{delay}} = 0$ fs), (b) advanced ($T_{\text{delay}} = 300$ fs), and (c) behind ($T_{\text{delay}} = -300$ fs) with respect to the FW pulse, respectively.

pulse dissociates the H_2^+ created by the advanced intense FW pulse through the $1\omega_{\text{SH}}$ pathway, leading to the H^+ emitting to $\phi_{H^+} = 0^\circ$ or $\phi_{H^+} = \pm 180^\circ$ in Fig. 3(c).

The emission dynamics of the H^+ can be controlled on attosecond time scale by adjusting the relative phase ϕ_L of the OTC pulse. One of the most interesting controls is the asymmetric emission of H^+ in the dissociative ionization of H_2 . To qualify it, we define the asymmetry parameter as $A(E_k, \phi_L, \phi_{H^+}) = [N(E_k, \phi_L, \phi_{H^+}) - N(E_k, \phi_L, \phi_{H^+} + \pi)] / [N(E_k, \phi_L, \phi_{H^+}) + N(E_k, \phi_L, \phi_{H^+} + \pi)]$, where $N(E_k, \phi_L, \phi_{H^+})$ is the H^+ yield at the proton kinetic-energy E_k , emission angle ϕ_{H^+} , and phase ϕ_L of the OTC pulse. The asymmetry parameter is positive for H^+ emitting to $\phi_{H^+} = \phi$ and negative for H^+ emitting to $\phi_{H^+} = \phi + \pi$. Figure 4(a) shows a two-dimensional map of the

asymmetry parameter as a function of ϕ_L and E_k for protons emitting to $45^\circ < \phi_{H^+} < 65^\circ$. Clear asymmetries are visible for both the low- E_k and high- E_k regions as a function of the laser phase ϕ_L . The asymmetry parameters versus ϕ_L integrated over H^+ kinetic energy intervals of 0.2–0.4 eV and 0.6–0.7 eV are plotted in the top panel of Fig. 4(a), which are fitted by using $A_0 \sin(\phi_L + \phi_{A_0})$ where A_0 is the asymmetry amplitude and ϕ_{A_0} is the phase. The asymmetry amplitudes are revealed to be $A_{0,\text{high-}E_k} = 20\% \pm 0.5\%$ at high- E_k and $A_{0,\text{low-}E_k} = 15\% \pm 0.5\%$ at low- E_k , respectively.

To verify the analysis above, we numerically simulate a two-channel time-dependent Schrödinger equation (atomic units are used throughout unless otherwise stated)

$$i \frac{\partial}{\partial t} \begin{pmatrix} \chi_g(y, z; t) \\ \chi_u(y, z; t) \end{pmatrix} = \begin{pmatrix} -\frac{1}{2\mu} \frac{\partial^2}{\partial y^2} - \frac{1}{2\mu} \frac{\partial^2}{\partial z^2} + V_g(y, z) & \mathbf{E}(t) \cdot \mathbf{D}(y, z) \\ \mathbf{E}(t) \cdot \mathbf{D}(y, z) & -\frac{1}{2\mu} \frac{\partial^2}{\partial y^2} - \frac{1}{2\mu} \frac{\partial^2}{\partial z^2} + V_u(y, z) \end{pmatrix} \begin{pmatrix} \chi_g(y, z; t) \\ \chi_u(y, z; t) \end{pmatrix},$$

where μ is the reduced nuclear mass, χ_g and χ_u are the two-dimensional nuclear wave packets corresponding to the electron in $1s\sigma_g^+$ and $2p\sigma_u^+$ states whose potential energy surfaces are V_g and V_u , respectively. Two nuclei sit on (y, z) and $(-y, -z)$ symmetrically, and $\mathbf{D}(y, z)$ is the dipole coupling matrix. The OTC field is written as $\mathbf{E}(t) = [E_{\text{FW}} \cos(\omega_{\text{FW}}t + \phi_{\text{FW}}) \mathbf{e}_z + E_{\text{SH}} \cos(2\omega_{\text{FW}}t + 2\phi_{\text{FW}} + \phi_L) \mathbf{e}_y] \sin^2(\pi t/\tau)$, $0 < t < \tau$, where ϕ_{FW} is the carrier-envelope phase of the FW pulse, and ϕ_L is the relative phase between the orthogonal FW and SH waves. The pulse duration τ equals 14 FW optical cycles. We note that the ϕ_{FW} is not locked in the experiment. To simulate it, we average over the ϕ_{FW} for each ϕ_L . By doing this, we smear out the contribution of ϕ_{FW} and extract the asymmetry induced solely by the relative phase ϕ_L . The peak intensities of the FW and SH pulses in the simulations are set to be 9×10^{13} and 9×10^{12} W/cm², respectively, and averaged over the focusing volume. We repeatedly launch four ground states of H_2 (separated by half cycle) onto the $1s\sigma_g^+$ potential surface by assuming H_2 is mainly ionized around several optical peaks in the middle of the FW pulse. We

then freely propagate such nuclear wave packet for about 100 fs to obtain the initial bounded nuclear wave packets [31] to be dissociated by the OTC pulse. For the given laser parameters, the estimated ionization probability is much smaller than the dissociation probability; hence, the above numerical model can well describe the main physics in our experiment. Figure 4(b) presents the simulated asymmetry as a function of ϕ_L and E_k . The numerical results are well comparable with the experimental measurements.

Figures 5(a) and 5(b) plot the measured amplitude A_0 and phase ϕ_{A_0} of the asymmetry versus the H^+ emission direction ϕ_{H^+} for the low- E_k and high- E_k regions, respectively. As compared to the one-dimensional stage where the asymmetry is along the polarization axis of the employed laser field [3–24], we here observe significant asymmetric emission of H^+ in the direction between the polarization axes of the FW and SH waves of the OTC pulse. As shown in Figs. 5(a) and 5(b), there is an angle shift of the ϕ_{H^+} -dependences of the asymmetry amplitude A_0 between the low- E_k and high- E_k regions. Rather than at $\phi_{H^+} = \pm 45^\circ$ or $\pm 135^\circ$, the asymmetry is favored when H^+ emits slightly

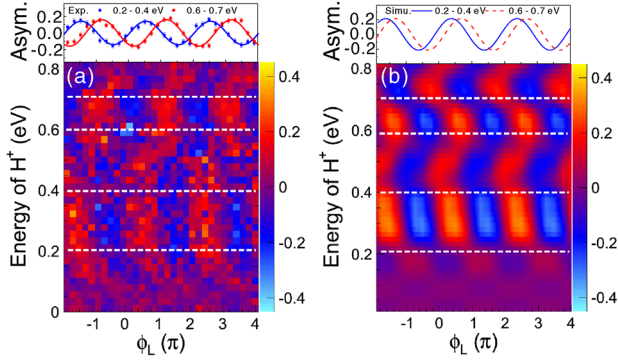


FIG. 4 (color online). The (a) experimentally measured and (b) numerically simulated two-dimensional maps of the asymmetry parameter as a function of ϕ_L and E_k for H^+ emitting to $45^\circ < \phi_{H^+} < 65^\circ$. The top panel shows the asymmetry parameter of the directional emission of H^+ versus ϕ_L at low- E_k and high- E_k regions as indicated between the dashed lines, fit to sinusoidal curves in (a).

close to the SH polarization ($\phi_{H^+} = 0^\circ$ or $\pm 180^\circ$) and FW polarization ($\phi_{H^+} = \pm 90^\circ$) for the low- E_k and high- E_k regions, respectively. The π -shift of the phase ϕ_{A_0} of the asymmetry for H^+ emitting to ϕ_{H^+} and $\phi_{H^+} + \pi$ validates our analysis and directly shows the directional dissociative ionization of H_2 in the phase-controlled OTC pulse. The numerically simulated A_0 and ϕ_{A_0} as a function of ϕ_{H^+} for the low- E_k and high- E_k regions are presented in Figs. 5(c) and 5(d), which are well comparable with the experiments. The measured two-dimensional maps of the amplitude A_0 and phase ϕ_{A_0} of the asymmetry parameter as a function of ϕ_{H^+} and E_k are displayed in Figs. 5(e) and 5(f).

The asymmetric directional emission of H^+ requires the coherent superposition of the nuclear wave packets with same kinetic energies but opposite parities [3–24] which must also overlap in the emission direction for the two-dimensional stage. By watching the numerical propagation of χ_g and χ_u , we may identify the dissociation pathways, as indeed depicted in Fig. 1(b). For the high- E_k region, χ_u comes from the $1\omega_{SH}$ pathway and χ_g comes from the net- $2\omega_{FW}$ pathway. By considering the dipole-allowed photon transitions parallel and perpendicular to the molecular axis [32], the angle-resolved asymmetry can be very nicely fitted with $\cos^2 \phi_{H^+} \sin^8 \phi_{H^+}$, as shown in Fig. 5(b) (solid curve). For the low- E_k region, χ_u comes from the $1\omega_{FW}$ pathway on the $2p\sigma_u^+$ curve, χ_g comes either from the $1\omega_{SH}-1\omega_{FW}$ pathway (propagation on the $1s\sigma_g^+$ curve undergoes one- ω_{SH} -photon transition to the $2p\sigma_u^+$ curve at point B, followed by propagation on the $2p\sigma_u^+$ curve and coupling back to the $1s\sigma_g^+$ curve at point C by emitting one ω_{FW} photon, followed by dissociation along the $1s\sigma_g^+$ curve) or from the $3\omega_{FW}-1\omega_{SH}$ pathway (propagation on the $1s\sigma_g^+$ curve undergoes three- ω_{FW} -photon transition to the $2p\sigma_u^+$ curve at point A, followed by propagation on the $2p\sigma_u^+$ curve and coupling back to the $1s\sigma_g^+$ curve at point B by emitting one ω_{SH} photon, followed by dissociation

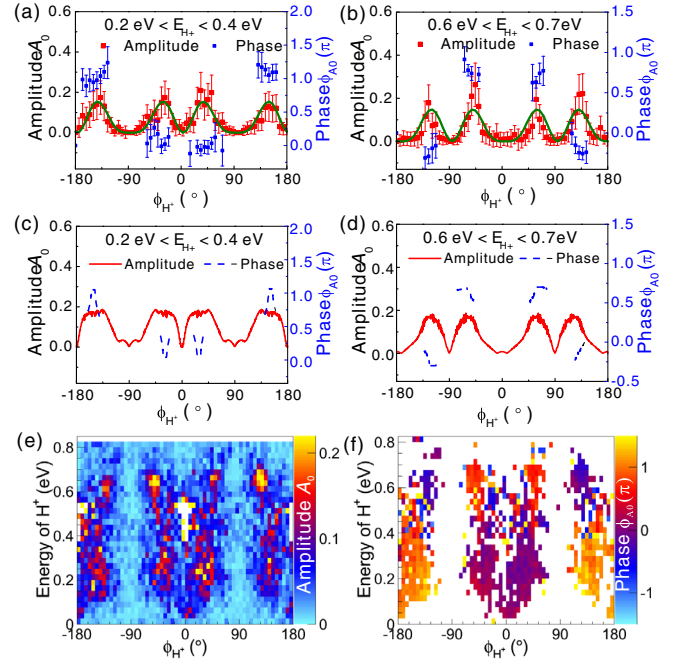


FIG. 5 (color online). The (a),(b) experimentally measured and (c),(d) numerically simulated asymmetry amplitude A_0 and phase ϕ_{A_0} as a function ϕ_{H^+} at (a, c) low- E_k and (b, d) high- E_k regions. The solid curves in (a),(b) are the fits of the angle-resolved asymmetry by assuming dipole-allowed photon transitions parallel and perpendicular to the molecular axis. The experimentally measured two-dimensional maps of the ϕ_{H^+} - E_k -dependent asymmetry amplitude A_0 and phase ϕ_{A_0} are displayed in (e) and (f).

along the $1s\sigma_g^+$ curve). As compared to the $1\omega_{SH}-1\omega_{FW}$ pathway, the $3\omega_{FW}-1\omega_{SH}$ pathway is energetically unfavored since four photons are required. It agrees with the relatively broader ϕ_{H^+} -dependence of the asymmetry amplitude A_0 of the low- E_k region [see Figs. 5(a) and 5(c)] as compared to the high- E_k region [see Figs. 5(b) and 5(d)]. For the high- E_k region, the four-photon-induced net- $2\omega_{FW}$ pathway leads to a narrow angular distribution by interfering with the $1\omega_{SH}$ pathway. Similar to the low- E_k region, as shown in Fig. 5(a) (solid curve), the angle dependence of the asymmetry at the high- E_k can be nicely fitted with $A_1 \cos^4 \phi_{H^+} \sin^2 \phi_{H^+} + A_2 \cos^8 \phi_{H^+} \sin^2 \phi_{H^+}$ [32], where $A_1 = 0.9 \pm 0.1$ and $A_2 = 0.2 \pm 0.2$ are the relative contributions of the $1\omega_{SH}-1\omega_{FW}$ and $3\omega_{FW}-1\omega_{SH}$ interference pathways, respectively. The observed $\sim \pi/2$ offset of the phase of the asymmetry of the low- E_k as compared to the high- E_k around the asymmetry peaks [see Figs. 5(a) and 5(b)] are considered in the fit.

In summary, we have observed emission-direction and kinetic-energy dependent asymmetric dissociative ionization of H_2 by using an intense phase-controlled OTC pulse. The underlying physics is understood to be the coherent superposition of the two-dimensional nuclear wave packets with opposite parities conjunctly driven by the FW and SH waves of the OTC pulse. Significant asymmetric proton

emission is observed in the direction between the polarization axes of the two colors of the OTC pulse. It stands for a two-dimensional steering of the nuclear wave packets or the localization of the remaining electron, which thus differs from the well-studied one-dimensional stage [3–24]. Our OTC strategy is applicable to a large class of molecules which paves the way to realize the control of molecular chemical reactions in a two-dimensional space.

We thank R. Dörner for helpful discussions. This work is supported by the National Natural Science Fund (Grants No. 11374103 and No. 11322438), the projects from Shanghai Science and Technology Commission (Grants No. 11ZR1417100 and No. 13QH1401400), the Eastern Scholar Program, and the Scholarship Award for Excellent Doctoral Student.

*fhe@sjtu.edu.cn

†hpzeng@phy.ecnu.edu.cn

‡jwu@phy.ecnu.edu.cn

- [1] A. Assion, T. Baumert, M. Bergt, T. Brixner, B. Kiefer, V. Seyfried, M. Strehle, and G. Gerber, *Science* **282**, 919 (1998).
- [2] M. Shapiro and P. Brumer, *Rep. Prog. Phys.* **66**, 859 (2003).
- [3] M. F. Kling, Ch. Siedschlag, A. J. Verhoef, J. I. Khan, M. Schultze, Th. Uphues, Y. Ni, M. Uiberacker, M. Drescher, F. Krausz, and M. J. J. Vrakking, *Science* **312**, 246 (2006).
- [4] M. Kremer, B. Fischer, B. Feuerstein, V. L. B. de Jesus, V. Sharma, C. Hofrichter, A. Rudenko, U. Thumm, C. D. Schröter, R. Moshhammer, and J. Ullrich, *Phys. Rev. Lett.* **103**, 213003 (2009).
- [5] B. Fischer, M. Kremer, T. Pfeifer, B. Feuerstein, V. Sharma, U. Thumm, C. D. Schröter, R. Moshhammer, and J. Ullrich, *Phys. Rev. Lett.* **105**, 223001 (2010).
- [6] J. McKenna, F. Anis, A. M. Saylor, B. Gaire, N. G. Johnson, E. Parke, K. D. Carnes, B. D. Esry, and I. Ben-Itzhak, *Phys. Rev. A* **85**, 023405 (2012).
- [7] H. Xu, T. Y. Xu, F. He, D. Kielpinski, R. T. Sang, and I. V. Litvinyuk, *Phys. Rev. A* **89**, 041403(R) (2014).
- [8] E. Charron, A. Giusti-Suzor, and F. H. Mies, *Phys. Rev. Lett.* **71**, 692 (1993).
- [9] B. Sheehy, B. Walker, and L. F. DiMauro, *Phys. Rev. Lett.* **74**, 4799 (1995).
- [10] H. Ohmura, N. Saito, and M. Tachiya, *Phys. Rev. Lett.* **96**, 173001 (2006).
- [11] D. Ray, F. He, S. De, W. Cao, H. Mashiko, P. Ranitovic, K. P. Singh, I. Znakovskaya, U. Thumm, G. G. Paulus, M. F. Kling, I. V. Litvinyuk, and C. L. Cocke, *Phys. Rev. Lett.* **103**, 223201 (2009).
- [12] K. J. Betsch, D. W. Pinkham, and R. R. Jones, *Phys. Rev. Lett.* **105**, 223002 (2010).
- [13] J. Wu, A. Vredenburg, L. Ph. H. Schmidt, T. Jahnke, A. Czasch, and R. Dörner, *Phys. Rev. A* **87**, 023406 (2013).
- [14] X. M. Tong and C. D. Lin, *Phys. Rev. Lett.* **98**, 123002 (2007).
- [15] V. Roudnev and B. D. Esry, *Phys. Rev. Lett.* **99**, 220406 (2007).
- [16] J. J. Hua and B. D. Esry, *J. Phys. B* **42**, 085601 (2009).
- [17] F. Kelkensberg, G. Sansone, M. Y. Ivanov, and M. Vrakking, *Phys. Chem. Chem. Phys.* **13**, 8647 (2011).
- [18] A. D. Bandrauk, S. Chelkowski, and H. S. Nguyen, *Int. J. Quantum Chem.* **100**, 834 (2004).
- [19] F. He, C. Ruiz, and A. Becker, *Phys. Rev. Lett.* **99**, 083002 (2007).
- [20] K. P. Singh, F. He, P. Ranitovic, W. Cao, S. De, D. Ray, S. Chen, U. Thumm, A. Becker, M. M. Murnane, H. C. Kapteyn, I. V. Litvinyuk, and C. L. Cocke, *Phys. Rev. Lett.* **104**, 023001 (2010).
- [21] G. Sansone, F. Kelkensberg, J. F. Pérez-Torres, F. Morales, M. F. Kling, W. Siu, O. Ghafur, P. Johnsson, M. Swoboda, E. Benedetti, F. Ferrari, F. Lépine, J. L. Sanz-Vicario, S. Zherebtsov, I. Znakovskaya, A. L’Huillier, M. Yu. Ivanov, M. Nisoli, F. Martín, and M. J. J. Vrakking, *Nature (London)* **465**, 763 (2010).
- [22] J. Wu, M. Magrakvelidze, L. P. H. Schmidt, M. Kunitski, T. Pfeifer, M. Schöffler, M. Pitzer, M. Richter, S. Voss, H. Sann, H. Kim, J. Lower, T. Jahnke, A. Czasch, U. Thumm, and R. Dörner, *Nat. Commun.* **4**, 2177 (2013).
- [23] T. Rathje, A. M. Saylor, S. Zeng, P. Wustelt, H. Figger, B. D. Esry, and G. G. Paulus, *Phys. Rev. Lett.* **111**, 093002 (2013).
- [24] N. G. Kling, K. J. Betsch, M. Zohrabi, S. Zeng, F. Anis, U. Ablikim, B. Jochim, Z. Wang, M. Kübel, M. F. Kling, K. D. Carnes, B. D. Esry, and I. Ben-Itzhak, *Phys. Rev. Lett.* **111**, 163004 (2013).
- [25] R. Dörner, V. Mergel, O. Jagutzki, L. Spielberger, J. Ullrich, R. Moshhammer, and H. Schmidt-Böcking, *Phys. Rep.* **330**, 95 (2000).
- [26] J. Ullrich, R. Moshhammer, A. Dorn, R. Dörner, L. Ph. H. Schmidt, and H. Schmidt-Böcking, *Rep. Prog. Phys.* **66**, 1463 (2003).
- [27] O. Jagutzki, A. Cerezo, A. Czasch, R. Dörner, M. Hattabaß, M. Huang, V. Mergel, U. Spillmann, K. Ullmann-Pfleger, Th. Weber, H. S. Böcking, and G. D. W. Smith, *IEEE Trans. Nucl. Sci.* **49**, 2477 (2002).
- [28] T. Nubbemeyer, K. Gorling, A. Saenz, U. Eichmann, and W. Sandner, *Phys. Rev. Lett.* **101**, 233001 (2008).
- [29] B. Manschwetus, T. Nubbemeyer, K. Gorling, G. Steinmeyer, U. Eichmann, H. Röttke, and W. Sandner, *Phys. Rev. Lett.* **102**, 113002 (2009).
- [30] M. Magrakvelidze, F. He, S. De, I. Bocharova, D. Ray, U. Thumm, and I. V. Litvinyuk, *Phys. Rev. A* **79**, 033408 (2009).
- [31] Th. Ergler, A. Rudenko, B. Feuerstein, K. Zrost, C. D. Schröter, R. Moshhammer, and J. Ullrich, *Phys. Rev. Lett.* **97**, 193001 (2006).
- [32] A. M. Saylor, P. Q. Wang, K. D. Carnes, B. D. Esry, and I. Ben-Itzhak, *Phys. Rev. A* **75**, 063420 (2007).